



PCCP

Understanding the influence of defects and surface chemistry on ferroelectric switching: A ReaxFF investigation of BaTiO₃

Journal:	<i>Physical Chemistry Chemical Physics</i>
Manuscript ID	CP-ART-05-2019-002955.R1
Article Type:	Paper
Date Submitted by the Author:	25-Jul-2019
Complete List of Authors:	Akbarian, Dooman; Pennsylvania State University, Mechanical Engineering Yilmaz, Dundar; Pennsylvania State University, Mechanical Engineering Cao, Ye; Oak Ridge National Laboratory Ganesh, Panchapakesan; Oak Ridge National Laboratory, Dabo, Ismaila; Pennsylvania State University, Department of Materials Science and Engineering and Materials Research Institute MUNRO, JASON; Pennsylvania State University, Department of Materials Science and Engineering and Materials Research Institute Van Ginhoven, Renee ; Air Force Research Laboratory Space Vehicles Directorate van Duin, Adri; The Pennsylvania State University, Mechanical Engineering

SCHOLARONE™
Manuscripts

Understanding the influence of defects and surface chemistry on ferroelectric switching: A ReaxFF investigation of BaTiO₃

Dooman Akbarian¹, Dundar E. Yilmaz,¹ Ye Cao², P. Ganesh^{2}, Ismaila Dabo³, Jason Munro³, Renee Van Ginhoven⁴ and Adri C. T. van Duin^{1*}*

¹ Department of Mechanical Engineering, Pennsylvania State University, University Park, Pennsylvania 16802, USA.

² Center for Nanophase Materials Sciences, Oak Ridge National Laboratory, Oak Ridge, Tennessee 37831, USA.

³ Department of Materials Science and Engineering and Materials Research Institute, The Pennsylvania State University, University Park, Pennsylvania 16802, USA.

⁴ Air Force Research Laboratory (AFRL), Kirtland AFB, New Mexico 87117, USA.

* Corresponding Author

Abstract

Ferroelectric materials such as barium titanate (BaTiO_3) have a wide range of applications in nano scale electronic devices due to their outstanding properties. In this study, we developed an easily extendable atomistic ReaxFF reactive force field for BaTiO_3 that can capture both its field- as well as temperature-induced ferroelectric hysteresis and corresponding changes due to surface chemistry and bulk defects. Using our force field, we were able to reproduce and explain a number of experimental observations: (1) existence of a critical thickness of 4.8 *nm* below which ferroelectricity vanishes in BaTiO_3 ; (2) migration and clustering of oxygen vacancies (OVs) in BaTiO_3 and reduction in the polarization and the curie temperature due to the OVs; (3) domain wall interaction with surface chemistry to influence ferroelectric switching and polarization magnitude. This new computational tool opens up a wide range of possibilities for making predictions for *realistic* ferroelectric interfaces in energy-conversion, electronic and neuromorphic systems.

Introduction

Ferroelectric perovskites such as barium titanate (BaTiO_3) have demonstrated a great potential for applications in nonvolatile memories, transducers, micro sensors and capacitors because of their unique properties such as spontaneous polarization, piezoelectric and pyroelectric effects, as well as large dielectric constants¹⁻⁵. Recent advances in making artificial oxide heterostructures has enabled designing electronically important functional oxide interfaces as well as ferroelectric-based memristor devices⁶⁻⁷. Previous experimental studies showed that particle size and defects/dopants can significantly affect the dielectric properties of ferroelectric materials⁸⁻¹¹. Extensive experimental efforts have been put into BaTiO_3 /polymer composites for the purpose of improving the dielectric properties by introducing high dielectric constant fillers and sol-gel method¹²⁻¹⁴. In order to design and optimize these devices, it is essential to obtain detailed, atomistic-scale insight of the BaTiO_3 ferroelectric perovskite. Currently, there are three approaches to model the ferroelectric behavior of BaTiO_3 : phenomenological, first-principles and force field-based methods. The phenomenological methods such as the Landau-Ginzburg-Devonshire (LGD) model describe the energy of the system as a polynomial expansion of polarization, strain, temperature, external electric field and the polarization of system based on the displacement of charges¹⁵⁻¹⁶. Phase-field model, which is based on the LGD description of the ferroelectric polarization, further considers the inhomogeneous system with domain-domain interactions and long range order elastic and electric fields¹⁷. Although these methods can simply describe the ferroelectric perovskites, they do not consider the atomic structure of the system. First-principles methods such as the density functional theory (DFT) are considered as the most accurate models which derive the electronic structures of ferroelectric materials based on the laws of quantum mechanics¹⁸⁻²¹. However, because of high computational costs these first-

principles methods can only be viable for relatively small length (~ 5 nm) and short time scales (~ 100 ps) restricting investigation of hysteresis loops, sequential phase transitions and domain wall motions that occur at longer length ($\sim 10 - 100$ nm)- and time ($> ns$)-scales. Force field based methods can provide the computational speed required to perform molecular dynamics (MD) simulations with system length and time scales sufficiently large to describe the full chemistry of the ferroelectric perovskites. Currently, there are three force field-based models available for ferroelectric perovskites including BaTiO₃: shell model, effective Hamiltonian model and bond-valence model. In the shell model, the valence electrons are a massless, charged shell linked to a massive charged core. In this empirical potential, the interaction between the core and shell was considered at the oxygen atoms, by harmonic and fourth-order terms for the core-shell interactions on the Ba-O planes, and the Ti-O bonds, respectively²²⁻²³. The shell model has been utilized in several MD studies to investigate the effects of oxygen vacancies (OVs), strain and film thickness on the polarization of BaTiO₃ nano-films²⁴⁻³². However, since a very low mass was specified to the shell, a very small MD time step (~ 0.4 fs) in the MD simulations using this potential is essential to obtain accurate results limiting the length and the time scales of the MD simulations. An *ab-initio* based effective Hamiltonian model was developed as a function of only a small number of degrees of freedom including a local soft-mode amplitude vector and a local strain tensor³³⁻³⁴. This method has been successfully applied to some ferroelectric materials such as BaTiO₃ to investigate their finite-temperature properties³⁵⁻³⁹. The bond-valence (BV) empirical potential for ferroelectric materials includes a bond-valence vector energy term measuring the unit cell asymmetry. This potential is based on the conservation principles of the bond valence and the bond valence vector, and it has been successfully parametrized for different ferroelectric materials including BaTiO₃⁴⁰⁻⁴⁴. Also, Goddard et al developed a potential that

allows charge flow through polarizable charges by an extended polarizable core-shell model⁴⁵. These models can be utilized successfully within a single ferroelectric formulation, however, they cannot straightforwardly be extended to investigate the interactions of ferroelectric materials in multi-material interfaces, and cannot handle chemical reactions. One of the widely used reactive force fields is the ReaxFF reactive force field, which combines a bond order/bond distance relationship with a polarizable charge description⁴⁶⁻⁴⁷. In the ReaxFF the connectivity of atoms is determined by bond orders based on the interatomic distances that are updated every time step, which allows for bonds breaking and formation during the simulation. Moreover, in ReaxFF the polarization effects are calculated using a geometry-dependent charge calculation procedure based on the electronegativity equalization method (EEM)⁴⁸ which plays a key role in the modeling of BaTiO₃. The nonbonded interactions such as van der Waals and Coulomb interactions are determined between every pair of atoms, irrespective of connectivity, and any excessive close-range nonbonded interactions are excluded by defining a shielding term⁴⁶⁻⁴⁷. ReaxFF has been successfully applied to a wide range of systems such as polymer, covalent, metallic, and metal oxide/hydride/carbide materials⁴⁹⁻⁵⁰.

The aim of the current work was first to develop a ReaxFF reactive force field for BaTiO₃, which would enable us, for example, to evaluate the influence of surface chemistry on ferroelectric response. Using this force field, we performed MD simulations to represent the phase transition sequence, ferroelectric and thermal hysteresis loops for the BaTiO₃ crystal structure.

Furthermore, we investigated the effects of sample thickness, OVs and water medium on the domain wall and material polarization.

Methods

The ReaxFF reactive force field for BaTiO₃ was developed by training against a DFT derived training set including equations of state for tetragonal and cubic BaTiO₃ phases, OV energies and their migration barriers and asymmetric-symmetric-asymmetric BaTiO₃ unit cell conversion. Additionally, the *Ti* and *Ba* metal data and TiO₂ and BaO oxide data⁵¹⁻⁵² were included in the ReaxFF training set, which extends the transferability of the developed force field to BaO and TiO₂ materials. We mainly focused on training our force field against the tetragonal and cubic phases since most of the electronic devices work in these phases. Figure 1 compares the ReaxFF and DFT results for volume/energy equations of state for ferroelectric and non-ferroelectric BaTiO₃ phases indicating that ReaxFF values are in very good agreement with the calculated DFT values. DFT calculations were performed using the SEQQUEST code with the generalized gradient functional as formulated by Perdew, Burke and Ernzerhof (PBE and $6 \times 6 \times 6$ *k*-point grid. Note that the current ReaxFF formulation was focused on the tetragonal and cubic phases, therefore, it cannot correctly predict the orthorhombic and rhombohedral phases to be lower in energy than the tetragonal phases.

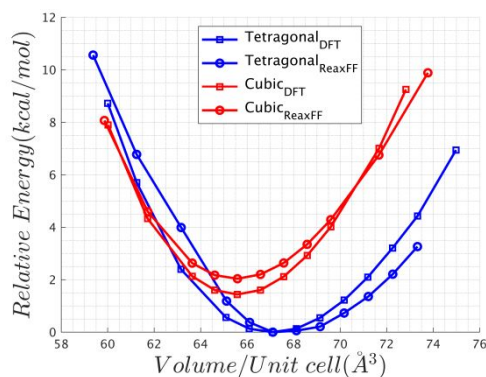


Figure 1. Comparison of DFT/PBE and ReaxFF equations of state for ferroelectric and non-ferroelectric BaTiO₃ crystal morphologies.

Also, ReaxFF estimates a +146.5 kcal/mol vacancy energy relative to O₂ for BaTiO₃, that is in good agreement with the corresponding DFT value of +182.6 kcal/mol considering that DFT

usually over-estimates the O₂ stability. Figure 2.a illustrates the lowest energy path for OV migration in BaTiO₃. As shown in Figure 2.a, ReaxFF predicts the energy barrier for OV migration very well (ReaxFF: 19.6 *kcal/mol*; DFT: 19.9 *kcal/mol*) which shows that ReaxFF should be capable of describing the OV migration and re-organization. The DFT calculations were performed using Vienna Ab initio Simulation Package (VASP) with the generalized gradient approximation (GGA) according to Perdew, Burke, and Ernzerhof revised for solids (PBEsol) and the projector augmented-wave method. Oxygen-vacancy formation energy calculations employed a 40-atom 2 × 2 × 2 as well as a 135-atom 3 × 3 × 3 supercell of BaTiO₃. The fully relaxed static transition energy barrier for a neutral oxygen vacancy was obtained employing the nudged elastic band method (NEB) where the residue NEB forces on the atoms were less than 0.05 eV/Å in a 2 × 2 × 2 supercell. A converged Γ point centered **k**-point mesh corresponding to 1.7 (1/Å) per atom was used for Brillouin zone integration and a plane wave energy cut off of 400 eV was used in all calculations. The structural relaxations were performed until the residual force of each atom was less than 0.01 eV/Å. Moreover, we could force a BaTiO₃ unit cell to transform from a tetragonal to a cubic structure using local restraints and based on DFT calculations, the barrier for this asymmetric to symmetric distortion is 2.1 *kcal/mol*; ReaxFF predicts a 2.0 *kcal/mol* barrier where the cubic state has the highest energy along the conversion path (Figure 2.b). The later DFT calculations were completed using the VASP with PBEsol functional, 6 × 6 × 6 *k*-point mesh, 600 eV plane-wave cutoff, and 1 × 10⁻⁶ eV energy error threshold.

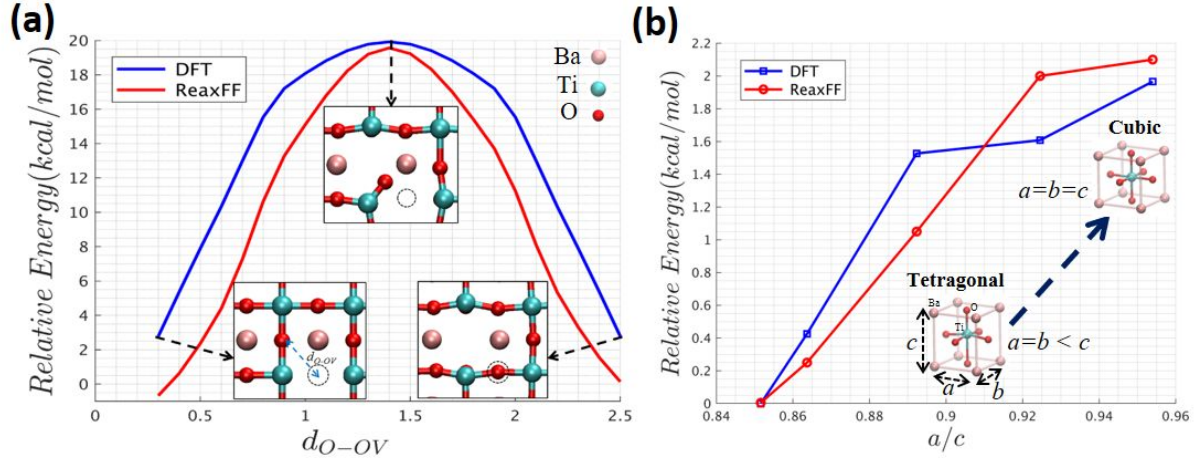


Figure 2. a): Comparison of DFT and ReaxFF energy barrier for OV migration. b): Comparison of DFT and ReaxFF energy for BaTiO₃ tetragonal to cubic phase conversion.

To derive the phase diagram and the thermal hysteresis loop of the BaTiO₃ crystal structure, *NPT-MD* simulations were carried out on a $6 \times 6 \times 6$ periodic BaTiO₃ supercell (Figure 3.a). For this purpose, the system was heated up, and subsequently cooled down both for 250 *ps* using a time step of 0.25 *fs* using a linear temperature regime in which $dT/dt = 0.002$ *K/fs* and the temperature was controlled by Berendsen thermostats and barostats with relatively weak coupling (100 *fs* for the thermostat, 2500 *fs* for the barostat coupling). The local polarization of each unit-cell $P_u(t)$ was defined as:

$$P_u(t) = \frac{1}{V_u} \left(Z_{Ti}^* r_{Ti}(t) + \frac{1}{8} Z_{Ba}^* \sum_{i=1}^8 r_{Ba,i}(t) + \frac{1}{2} Z_O^* \sum_{i=1}^6 r_{O,i}(t) \right)$$

where V_u is the volume of the unit cell Z_{Ti}^* , Z_{Ba}^* and Z_O^* are the charges of the *Ti*, *Ba* and *O* atoms obtained using the Electron Equilibration Method (EEM) approach in ReaxFF, and $r_{Ti,i}(t)$, $r_{Ba,i}(t)$ and $r_{O,i}(t)$ are the positions of the *Ti*, *Ba* and *O* atoms of each unit cell at time t .

Results and Discussion

Figure 3.b shows that ReaxFF can successfully reproduce the tetragonal and cubic phases with a phase transition temperature at $T_c = 240$ K. Figure 3.c shows the total polarization of the system

for the heat up/cool down cycle, in which the hysteresis of the phase transition confirms the first-order nature of the cubic-to-tetragonal phase transition. As Figure 3.d shows, below 240 K, the polarization of each unit cell is along the [010] direction ($P_x = P_z = 0, P_y > 0$) which is characteristic of the tetragonal phase. Our potential only considers the tetragonal and cubic phases, however, this does not affect the practical application of the ReaxFF potential since these are the phases that are relevant for most of the applications of this materials and these phases are the main ones related to the working conditions of electronic devices.

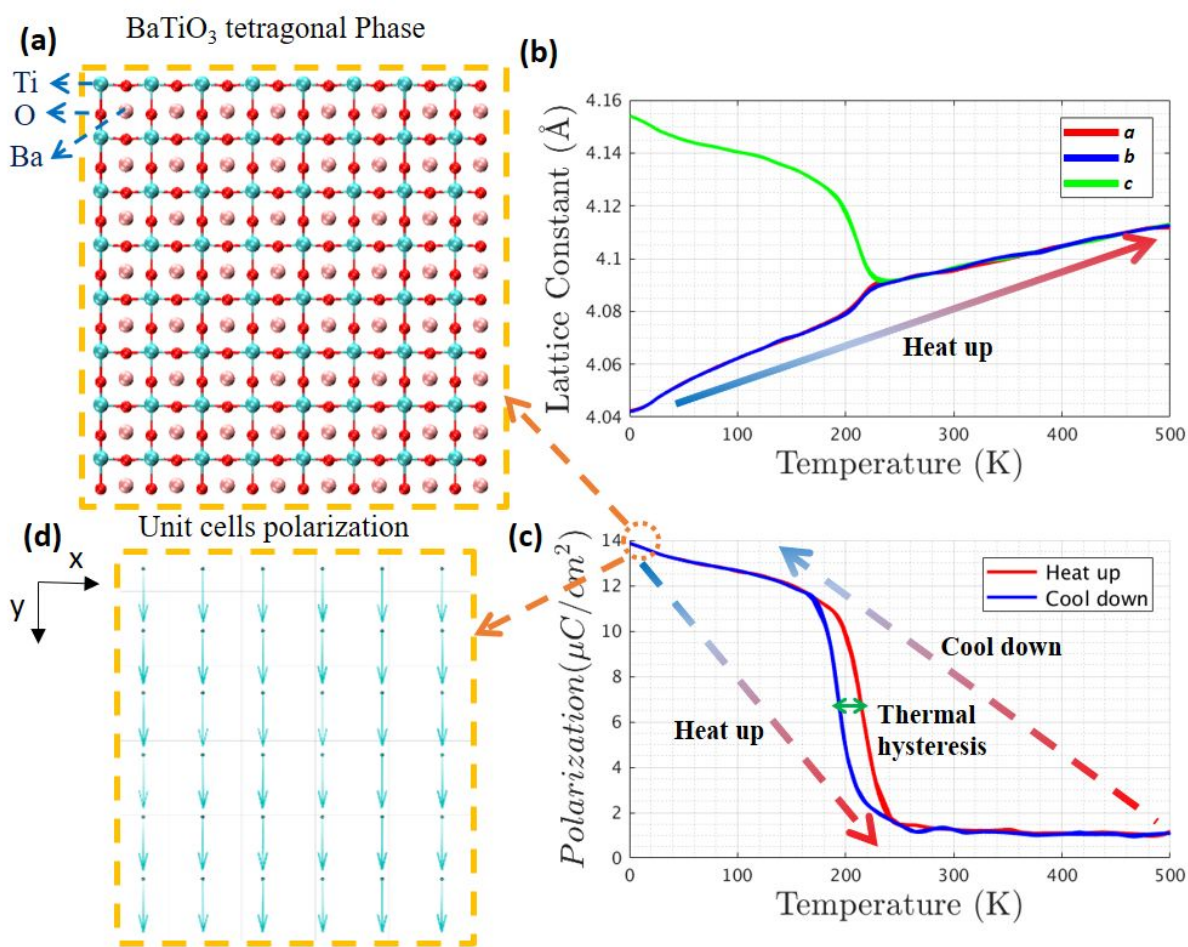


Figure 3. a) The $6 \times 6 \times 6$ periodic BaTiO₃ supercell. b) Temperature dependence of the lattice constants with the phase transition from tetragonal to cubic at 240K. c) Total polarization vs temperature showing the first-order nature of the cubic-to-tetragonal phase transition. d) demonstration of unit cell polarizations in tetragonal phase in which they are all aligned in one direction.

The ferroelectric/non-ferroelectric phase transition temperature predicted by ReaxFF is closer to the experimental value compared to the calculated values by other potentials such as the shell and bond valence model listed in Table 1. The ferroelectric/non-ferroelectric phase transition temperature predicted by all potentials listed in Table 1 are underestimated since the precision of DFT methods depends on the exchange-correlation functionals and almost all DFT calculations underestimate the energy barriers between states of different phases^{40, 53-54}. Moreover, we observe that ReaxFF generally predicts a lower energy than DFT along the tetragonal to cubic phase conversion path (Figure 2.b), which could explain why a lower phase transition temperature is predicted by ReaxFF compared to the reference values reported in Table 1. Also, the lattice constants and spontaneous polarization predicted by ReaxFF are in good agreement with the values obtained by experimental and numerical/theoretical methods (Table 1).

Table 1. Comparison of lattice constants and unit cell polarization of BaTiO₃ tetragonal and cubic phases predicted by ReaxFF with DFT, experiment and other potentials.

Parameter		Shell ²³	BV ⁴⁰	ReaxFF	Experiment	DFT		
Lattice constants (Å)	Tetragonal	<i>a=b</i>	4.002	4.005	4.041	3.999 ⁵⁵	Literature 3.966 ⁵⁶ , 3.943 ⁵⁷ , 3.985 ⁴⁰	Our work 4.024
			<i>c</i>	4.043	4.109	4.155	4.036 ⁵⁵	4.035 ⁵⁶ , 3.994 ⁵⁷ , 4.089 ⁴⁰
	Cubic	<i>a</i>	4.016	4.037	4.091	4.012 ⁵⁸ , 4.000 ⁵⁹	4.002 ⁴⁰	4.033
<i>P_s</i> (μC/cm²)		17	28	14	26 ⁶⁰ , 27 ⁶¹ , 17 ⁵⁵	22.9 ⁵⁷ , 29 ⁵⁶		
<i>T_c</i> (K)		160	160	240	393 ⁵³			

Due to the rapid and continuous demand for miniaturization of electronic devices, the technology of ferroelectrics moved toward thin nanometer scale films^{1, 62-63}. However, the reduction of the ferroelectric size to the nanoscale significantly affects the polarization which limits the

miniaturization process⁶²⁻⁶³. Investigations on the physics of ultrathin ferroelectric films and specially the critical size for ferroelectricity have attracted significant attention^{35-36, 62-65}. It was thought for a long time that ferroelectricity was suppressed in ultrathin films, and samples below a critical size of few tens of nanometers could not sustain a spontaneous polarization⁶², however, recent experimental and numerical studies could identify ferroelectricity in much thinner films than previously thought^{63, 66-67}. In our study, we used our developed force field for BaTiO₃ to first derive the ferroelectric hysteresis loop by applying an electric field on a BaTiO₃ slab with [0 0 1] surfaces and then identify the minimum thickness required to observe the ferroelectricity. Figure 4 depicts the hysteresis loops obtained by applying electric field on BaTiO₃ slabs with different thicknesses. The hysteresis loops for films thicker than 4.8 nm clearly show the remnant polarization, the saturation polarization, and the reversal electric field which are characteristics of a ferroelectric material. The results reveal the thickness dependency of the polarization in BaTiO₃ thin films. Based on our results a minimum thickness of 4.8 nm is required to observe the ferroelectric hysteresis effect which is in very good agreement with the 4.4 nm value found by experimental investigations⁶⁷.

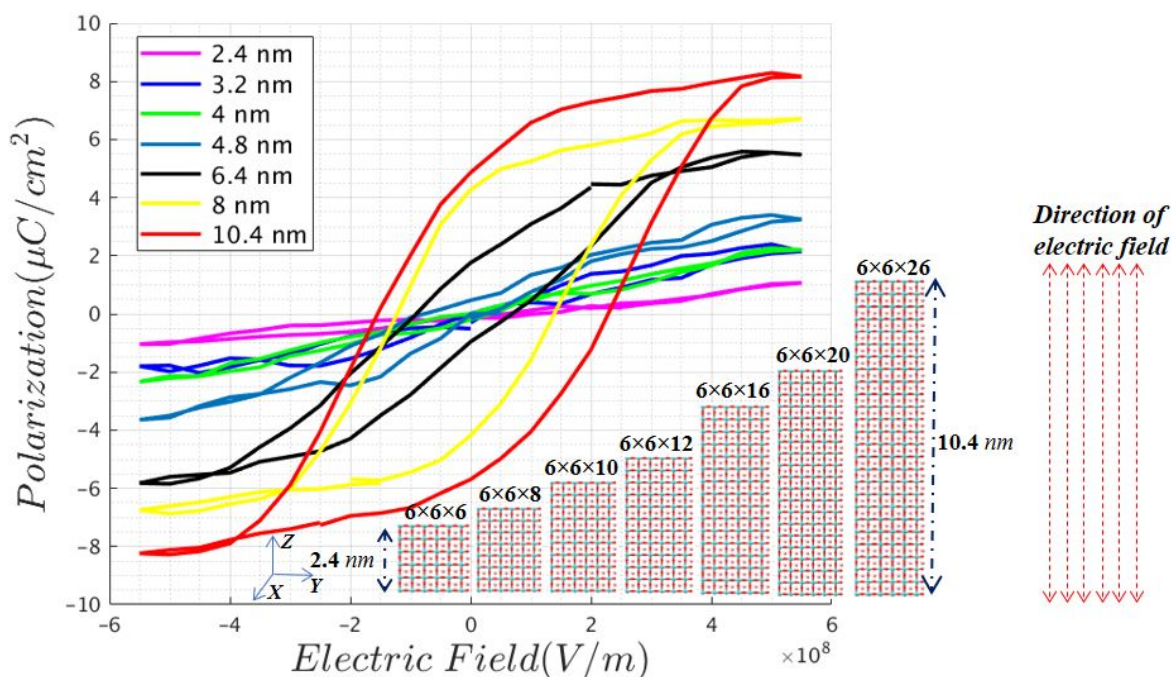


Figure 4. The hysteresis loop obtained by applying electric field on the BaTiO₃ slabs with different thickness. A minimum thickness of 4.8 nm is required to observe the ferroelectric hysteresis effect.

Vacancies can significantly affect the behavior and performance of ferroelectrics in capacitors, memories, and energy conversion devices⁶⁸⁻⁶⁹. Particularly, defects can deteriorate the polarization and cause fatigue after frequent polarization switching^{68, 70}. However, defects sometimes can cause useful properties that do not exist in pure crystals⁷¹⁻⁷². For instance, appropriate concentration of vacancies can increase the conductivity in SrTiO₃ which is otherwise difficult to achieve by other methods^{71, 73-74}. Also, using defect mediated reversible domain switching in aged BaTiO₃, large recoverable strain under low electric field can be generated⁷². The lack of an accurate and computationally inexpensive method which can reliably predict the physical properties of defective BaTiO₃ has hampered further progress, especially for large length and time scales phenomena. In this study, we used our developed force field to find how the OVs in BaTiO₃ interact with each other by running *NPT-MD* simulation at 1000K on a $6 \times 6 \times 6$ periodic BaTiO₃ supercell including 5 OVs. As Figure 5.a shows, the OVs were initially

at least 12 (Å) away from each other, however, after running the simulation for 2.25 ns, the OV's attracted each other and tend to form a cluster (Figure 5.b). Previous studies also reported that OV's in barium strontium cobalt iron oxide (BSCF) tend to form cluster arrangements⁷⁵.

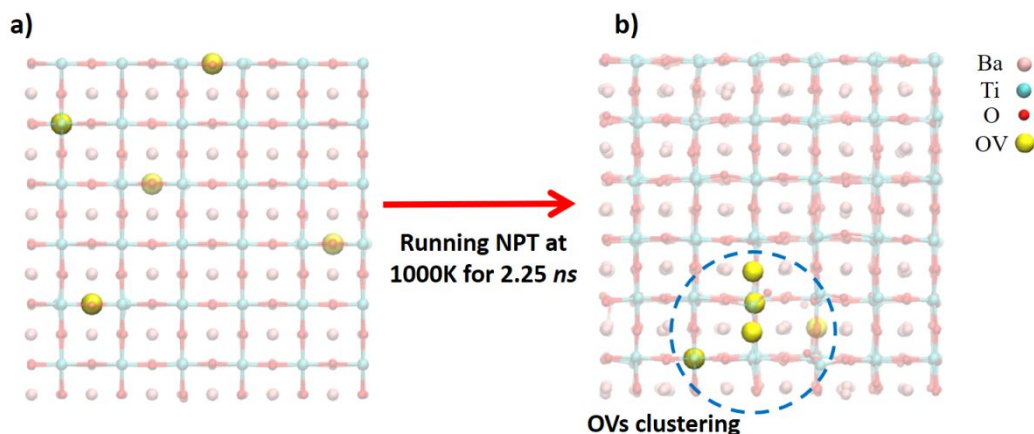


Figure 5. (a) OV's were designed to be at least 12 (Å) far from each other. (b) clustering of OV's after running NPT-MD simulation at 1000K for 2.25 ns.

Also, we evaluated the vacancy formation energetics in cubic BaTiO₃ as a further verification of the BaTiO₃ ReaxFF force field. We calculated the formation energies of the oxygen, barium and titanium vacancies using the following equation:

$$E_f^d = E^{defected} - E^{pristine} - \sum_{i=Ba, Ti, O} \mu_i N_i$$

where $E^{defected}$ and $E^{pristine}$ are the total energy of the defective and reference systems, respectively, and N_i terms shows the difference in the number of *Ba*, *Ti* and *O* atoms in the defected and pristine structures and μ_i terms represent the chemical potentials of *Ba*, *Ti* and *O* atoms referenced to *Ba bcc* lattice, *Ti hcp* lattice and the *O*₂ dimer, respectively. Table 2 compares the calculated defect formation energies of *Ba*, *Ti* and *O* defects within ReaxFF and the DFT values reported by Erhart et al⁷⁶., showing very good agreement. Also, as listed on Table 2 the calculated chemical potentials by ReaxFF for *Ba*, *Ti* and *O* atoms are -1.73, -4.98, -2.8 eV/atom, in close agreement with the experimental values of -1.87 eV/atom for *Ba*, -4.85

$eV/atom$ for Ti and $-2.58 eV/atom$ for O^{76} . Based on the results, the oxygen vacancy (OV) is the most energetically favorable defect which can happen even at room temperature.

Table 2. Defect formation energies and chemical potentials predicted by ReaxFF compared with DFT and experimental values.

	Formation Energy (eV/mol)				Chemical Potential ($eV/atom$)		
	E_f^O	E_f^{Ba}	E_f^{Ti}		μ_{Ba}	μ_{Ti}	μ_O
<i>ReaxFF</i>	9.07	9.80	17.94	<i>ReaxFF</i>	-1.73	-4.98	-2.8
<i>DFT</i> ⁷⁶	8.22	10.25	14.55	<i>Experiment</i> ⁷⁶	-1.87	-4.85	-2.58

Moreover, we used our developed force field to investigate the effects of different concentration of OVs on the initial polarization and the phase transition temperature. Table 3 shows the effects of the OVs on the initial polarization (P_i) and the phase transition temperature (T_c). Based on our findings, by increasing the OV concentration in the system, the phase transition temperature and the initial polarization decrease monotonically. For instance, 0.5 % and 1.0 % OV in the system decrease the initial polarization from the initial value of $14 \mu C/cm^2$ to $12.95 \mu C/cm^2$ and $11.52 \mu C/cm^2$, respectively, and the phase transition temperature from 240 K to 180 K and 150 K. Other MD and *ab-initio* studies also observed that OVs decrease the phase transition temperature and the initial polarization of the $BaTiO_3$ structure^{27, 32, 77}. OV induced polarization loss in ferroelectrics is because OVs distort the polarization of the unit cells, therefore, the polarization of such unit cells can be hardly rectified in the original direction³². Moreover, the polarization can be pinned to a specific direction by OVs which leads to tail-to-tail polarizations along the Ti - OV - Ti pattern and suppression of the total polarization⁷⁷.

Table 3. The effect of the OVs on the initial polarization and the phase transition temperature.

% OV	P_i ($\mu C/cm^2$)	T_c (K)
0	14	240
0.5	12.95	180
1	11.52	150
1.5	10.54	140
2	7.80	130

Ferroelectrics are composed of domains of different polarization orientations, separated by domain walls. The normal component of spontaneous polarization is usually continuous across the domain walls to minimize the polarization charges ($-\nabla \cdot P$) and meet the electrostatic compatibility condition⁷⁸. These are called neutral domain walls (NDW) as they exhibit no net bound charges. On the other hand, charged domain walls (CDW) exhibit net polarization bound charges due to the discontinuity of polarizations across the domain walls⁷⁸. Figure 6.a shows the capability of ReaxFF to predict a head-to-head 180° charged domain wall formation in a 14.4 nm thick BaTiO_3 slab with $\text{TiO}_2 [0 0 1]$ surfaces. Due to $\text{TiO}_2 [0 0 1]$ surfaces, negative unscreened bound charges exist on the surfaces of the BaTiO_3 slab creating a charged domain wall in the middle of the slab which violates the condition of electrostatic compatibility⁷⁸. This observation indicates that our force field can be utilized to study the complex dynamics of domain walls in BaTiO_3 .

Uniquely, ReaxFF allows us to evaluate the effects of surface chemistry on domain wall structure and mobility. Water molecules are easily adsorbed on BaTiO_3 surfaces and change their physical properties. Therefore, the atomistic scale study of the water adsorption on ferroelectric surfaces is crucial for the advance in the understanding of BaTiO_3 ferroelectrics properties and can benefit the associated applications⁷⁹⁻⁸⁰. Previous investigations indicated that the charge screening induced by molecular adsorbates such as hydroxyl, carboxylate and oleic acid can stabilize the ferroelectricity and decrease the critical size in BaTiO_3 nanowires and nanoparticles^{20, 81}. We utilized our developed force field to investigate the effects of a water medium on the polarization of a 14.4 nm thick BaTiO_3 slab with $\text{TiO}_2 [0 0 1]$ surfaces, by adding water molecules around surfaces and running MD simulations for 0.5 ns . As Figure 6.b shows, the water molecules are adsorbed on the surfaces and dissociated into hydroxyl groups.

Therefore, surfaces are screened by the adsorption of water molecules on the surfaces causing the polarization rearrangement in the BaTiO₃ slab⁸². As Figure 6 shows, adding water molecules leads to an increased amount of polarization from 4.6 $\mu\text{C}/\text{cm}^2$ to 12.5 $\mu\text{C}/\text{cm}^2$ due to the charge screening induced by adsorption of water molecules on the surfaces of BaTiO₃ slab⁸².

Additionally, as Figure 6.b shows, dissociative adsorption of water molecules on the surfaces leads to a 90° domain switching compared to Figure 6.a in which domains are aligned in the z direction. Such an observation was reported by Li et al. in which using *ab-initio* method they showed that when the water molecules are dissociatively adsorbed on the TiO₂ terminated surfaces, a 90° surface domain switching occurs⁸². Our results indicate that our developed force field can be successfully used to study the interactions of BaTiO₃ in multi-material interfaces and its related applications.

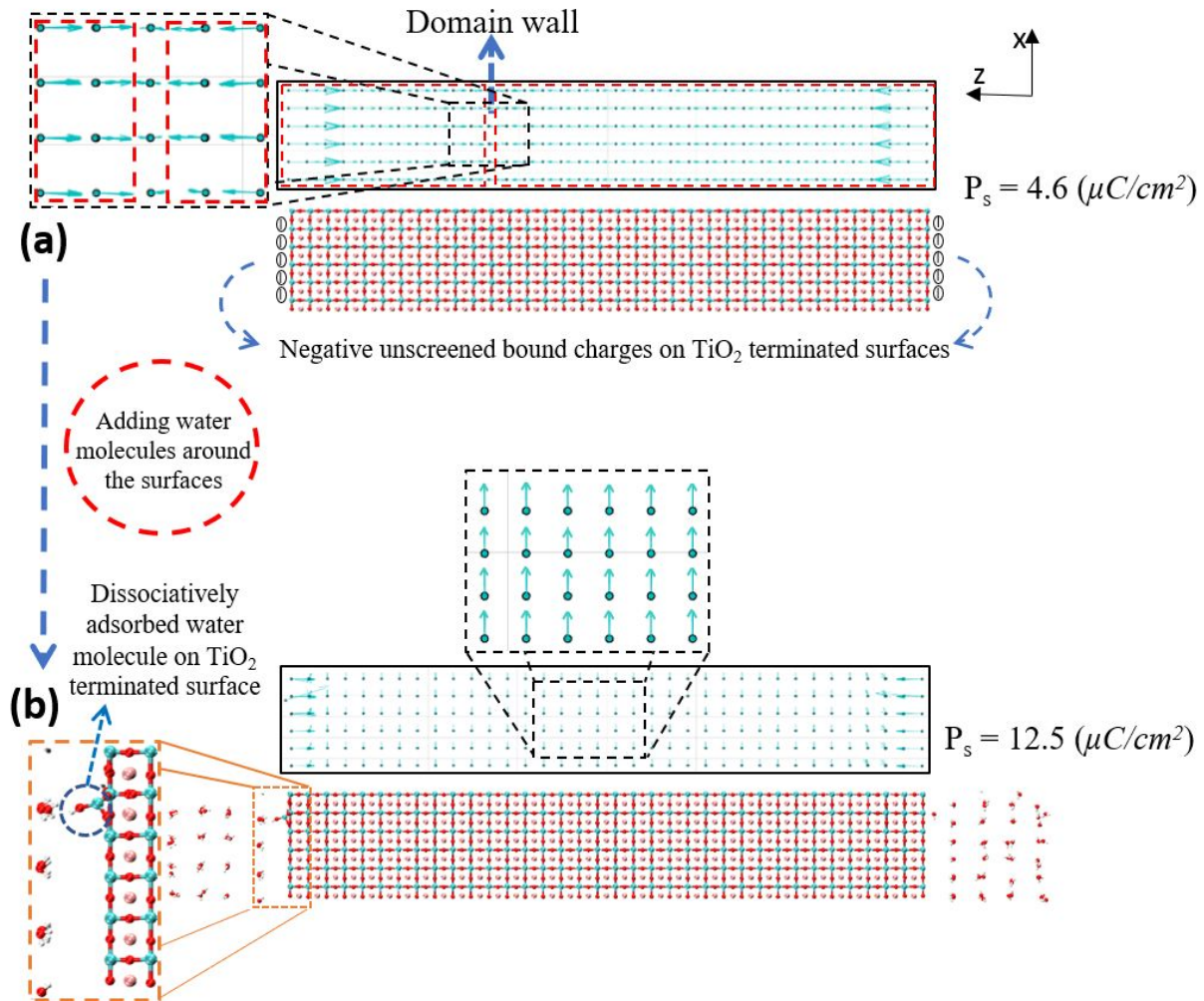


Figure 6. (a) Demonstration of a head-to-head 180° charged domain wall formation in a 14.4 nm thick BaTiO₃ slab with TiO₂ [0 0 1] surfaces. Due to TiO₂ [0 0 1] surfaces, negative unscreened bound charges exist on the surfaces of the BaTiO₃ slab creating a charged domain wall near the middle of the slab. (b) Adding water molecules around the surfaces leads to an increased amount of polarization from $4.6 \text{ } (\mu\text{C}/\text{cm}^2)$ to $12.5 \text{ } (\mu\text{C}/\text{cm}^2)$ due to the charge screening induced by adsorption of water molecules on the surfaces. Moreover, this leads to a 90° domain switching compared to the surface condition in Figure 6.a in which domains are aligned in the z direction.

Conclusion

As a conclusion, we successfully developed the ReaxFF description to the ferroelectric and non-ferroelectric phases for BaTiO₃. This extension was performed without any modification in the ReaxFF functional form which means that this BaTiO₃ parameter set can be straightforwardly extended to a wide range of other ferroelectric oxides, including those with crystal phase stabilities that are highly sensitive to defects and strain, such as orthorhombic HfO₂/ZrO₂, providing a unique and computationally inexpensive simulation tool for realistic ferroelectric

materials. OV's and their migration were also considered in the force field development. Given that realistic BaTiO₃ materials have a significant concentrations of defects, this again extends the realism of the ReaxFF description. We tested the ReaxFF BaTiO₃ parameter set in a series of MD simulation, which reproduced a reversible ferroelectric/non-ferroelectric phase transition upon heating and cooling. Using our developed force field, we found a minimum thickness of 4.8 nm is required to observe the ferroelectric hysteresis effect. Also, we indicated that OV's in BaTiO₃ tend to form a cluster and reduce the polarization and the phase transition temperature. Moreover, the BaTiO₃ ReaxFF reactive force field has the capability of predicting the dynamics of neutral and charged domain walls in BaTiO₃. Finally, we found that charge screening induced by adsorption of water molecules on the TiO₂ terminated surfaces of a BaTiO₃ slab leads to a 90° domain switching and an increased amount of polarization comparing to a BaTiO₃ slab with unscreened TiO₂ terminated surfaces. The satisfactory comparison of the ReaxFF results with available experimental and *ab-initio* data indicates the robustness and capabilities of the new ReaxFF reactive potential. Our encouraging results should allow us to further investigate the role of such point-defects on domain-motion, switching and piezoelectric and other linear as well as non-linear field-responses using the ReaxFF force-field formalism, and this can be tremendously useful for a wide range of technological applications involving ferroelectric interfaces in energy-conversion, electronic and neuromorphic systems.

Acknowledgements We acknowledge funding from AFRL grant FA9451-16-1-0041. PG was supported by the Center for Nanophase Materials Sciences (CNMS), which is a US DOE Office of Science User Facility, located at Oak Ridge National Laboratory. J.M.M. and I.D. acknowledge support from the Natural Sciences and Engineering Research Council of Canada (NSERC) and the National Science Foundation under Grant No. 1807768, respectively.

References

1. Rabe, K. M.; Ahn, C. H.; Triscone, J.-M., *Physics of ferroelectrics: a modern perspective*. Springer Science & Business Media: 2007; Vol. 105.
2. Xu, Y., *Ferroelectric materials and their applications*. Elsevier: 2013.
3. Cross, L. E., Ferroelectric materials for electromechanical transducer applications. *Materials chemistry and physics* **1996**, *43* (2), 108-115.
4. Bowen, C.; Kim, H.; Weaver, P.; Dunn, S., Piezoelectric and ferroelectric materials and structures for energy harvesting applications. *Energy & Environmental Science* **2014**, *7* (1), 25-44.
5. Setter, N.; Damjanovic, D.; Eng, L.; Fox, G.; Gevorgian, S.; Hong, S.; Kingon, A.; Kohlstedt, H.; Park, N.; Stephenson, G., Ferroelectric thin films: Review of materials, properties, and applications. *Journal of Applied Physics* **2006**, *100* (5), 051606.
6. Zhang, Y.; Lu, H.; Xie, L.; Yan, X.; Paudel, T. R.; Kim, J.; Cheng, X.; Wang, H.; Heikes, C.; Li, L., Anisotropic polarization-induced conductance at a ferroelectric–insulator interface. *Nature nanotechnology* **2018**, *13* (12), 1132.
7. Chanthbouala, A.; Garcia, V.; Cherifi, R. O.; Bouzehouane, K.; Fusil, S.; Moya, X.; Xavier, S.; Yamada, H.; Deranlot, C.; Mathur, N. D., A ferroelectric memristor. *Nature materials* **2012**, *11* (10), 860.
8. Rumpf, H.; Modrow, H.; Hormes, J.; Gläsel, H.-J.; Hartmann, E.; Erdem, E.; Böttcher, R.; Hallmeier, K.-H., Preparation of nanocrystalline BaTiO₃ characterized by in situ X-ray absorption spectroscopy. *The Journal of Physical Chemistry B* **2001**, *105* (17), 3415-3421.
9. Erdem, E.; Semmelhack, H.-C.; Böttcher, R.; Rumpf, H.; Banys, J.; Matthes, A.; Gläsel, H.-J.; Hirsch, D.; Hartmann, E., Study of the tetragonal-to-cubic phase transition in PbTiO₃ nanopowders. *Journal of Physics: Condensed Matter* **2006**, *18* (15), 3861.
10. Erdem, E.; Jakes, P.; Parashar, S.; Kiraz, K.; Somer, M.; Rüdiger, A.; Eichel, R.-A., Defect structure in aliovalently-doped and isovalently-substituted PbTiO₃ nano-powders. *Journal of Physics: Condensed Matter* **2010**, *22* (34), 345901.
11. Erdem, E.; Kiraz, K.; Somer, M.; Eichel, R.-A., Size effects in Fe³⁺-doped PbTiO₃ nanocrystals—Formation and orientation of (FeTi³⁺VO) defect-dipoles. *Journal of the European Ceramic Society* **2010**, *30* (2), 289-293.
12. Bi, M.; Hao, Y.; Zhang, J.; Lei, M.; Bi, K., Particle size effect of BaTiO₃ nanofillers on the energy storage performance of polymer nanocomposites. *Nanoscale* **2017**, *9* (42), 16386-16395.
13. Suematsu, K.; Arimura, M.; Uchiyama, N.; Saita, S.; Makino, T., High-performance dielectric thin film nanocomposites of barium titanate and cyanoethyl pullulan: controlling the barium titanate nanoparticle size using a sol–gel method. *RSC Advances* **2016**, *6* (25), 20807-20813.
14. Jiang, B.; Iocozzia, J.; Zhao, L.; Zhang, H.; Harn, Y.-W.; Chen, Y.; Lin, Z., Barium titanate at the nanoscale: controlled synthesis and dielectric and ferroelectric properties. *Chemical Society Reviews* **2019**, *48* (4), 1194-1228.
15. Devonshire, A. F., XCVI. Theory of barium titanate: Part I. *The London, Edinburgh, and Dublin Philosophical Magazine and Journal of Science* **1949**, *40* (309), 1040-1063.
16. Devonshire, A. F., CIX. Theory of barium titanate—Part II. *The London, Edinburgh, and Dublin Philosophical Magazine and Journal of Science* **1951**, *42* (333), 1065-1079.
17. Chen, L. Q., Phase-field method of phase transitions/domain structures in ferroelectric thin films: a review. *Journal of the American Ceramic Society* **2008**, *91* (6), 1835-1844.
18. Cohen, R.; Krakauer, H., Lattice dynamics and origin of ferroelectricity in BaTiO₃: Linearized-augmented-plane-wave total-energy calculations. *Physical Review B* **1990**, *42* (10), 6416.
19. Piskunov, S.; Heifets, E.; Eglitis, R.; Borstel, G., Bulk properties and electronic structure of SrTiO₃, BaTiO₃, PbTiO₃ perovskites: an ab initio HF/DFT study. *Computational Materials Science* **2004**, *29* (2), 165-178.

20. Spanier, J. E.; Kolpak, A. M.; Urban, J. J.; Grinberg, I.; Ouyang, L.; Yun, W. S.; Rappe, A. M.; Park, H., Ferroelectric phase transition in individual single-crystalline BaTiO₃ nanowires. *Nano letters* **2006**, *6* (4), 735-739.
21. Kolpak, A. M.; Li, D.; Shao, R.; Rappe, A. M.; Bonnell, D. A., Evolution of the structure and thermodynamic stability of the BaTiO₃ (001) surface. *Physical review letters* **2008**, *101* (3), 036102.
22. Khatib, D.; Migoni, R.; Kugel, G.; Godefroy, L., Lattice dynamics of BaTiO₃ in the cubic phase. *Journal of Physics: Condensed Matter* **1989**, *1* (49), 9811.
23. Tinte, S.; Stachiotti, M.; Sepiarsky, M.; Migoni, R.; Rodriguez, C., Atomistic modelling of BaTiO₃ based on first-principles calculations. *Journal of Physics: Condensed Matter* **1999**, *11* (48), 9679.
24. Tinte, S.; Stachiotti, M.; Sepiarsky, M.; Migoni, R.; Rodriguez, C., Order-disorder, local structure and precursor effects in BaTiO₃. *Ferroelectrics* **2000**, *237* (1), 41-48.
25. Tinte, S.; Stachiotti, M. G., Surface effects and ferroelectric phase transitions in BaTiO₃ ultrathin films. *Physical Review B* **2001**, *64* (23).
26. Sepiarsky, M.; Tinte, S., Dynamical behavior of the phase transition of strained from atomistic simulations. *Physica B: Condensed Matter* **2009**, *404* (18), 2730-2732.
27. Chen, Y.; Liu, B.; Ma, Y.; Zhou, Y., Modification of a shell model for the study of the radiation effects in BaTiO₃. *Nuclear Instruments and Methods in Physics Research Section B: Beam Interactions with Materials and Atoms* **2009**, *267* (18), 3090-3093.
28. Gonçalves, L. G. V.; Rino, J. P., Finite size effects on a core-shell model of barium titanate. *Computational Materials Science* **2017**, *130*, 98-102.
29. Zhang, Y.; Hong, J.; Liu, B.; Fang, D., Strain effect on ferroelectric behaviors of BaTiO₃ nanowires: a molecular dynamics study. *Nanotechnology* **2010**, *21* (1), 015701.
30. Zhang, Y.; Hong, J.; Liu, B.; Fang, D., Molecular dynamics investigations on the size-dependent ferroelectric behavior of BaTiO₃ nanowires. *Nanotechnology* **2009**, *20* (40), 405703.
31. Sang, Y.; Liu, B.; Fang, D., The size and strain effects on the electric-field-induced domain evolution and hysteresis loop in ferroelectric BaTiO₃ nanofilms. *Computational Materials Science* **2008**, *44* (2), 404-410.
32. Wang, J.; Shen, Y.; Song, F.; Ke, F.; Bai, Y.; Lu, C., Effects of oxygen vacancies on polarization stability of barium titanate. *Science China Physics, Mechanics & Astronomy* **2016**, *59* (3).
33. Zhong, W.; Vanderbilt, D.; Rabe, K. M., Phase transitions in BaTiO₃ from first principles. *Phys Rev Lett* **1994**, *73* (13), 1861-1864.
34. Zhong, W.; Vanderbilt, D.; Rabe, K., First-principles theory of ferroelectric phase transitions for perovskites: The case of BaTiO₃. *Physical Review B* **1995**, *52* (9), 6301.
35. Paul, J.; Nishimatsu, T.; Kawazoe, Y.; Waghmare, U. V., Ferroelectric phase transitions in ultrathin films of BaTiO₃. *Phys Rev Lett* **2007**, *99* (7), 077601.
36. Nishimatsu, T.; Waghmare, U. V.; Kawazoe, Y.; Vanderbilt, D., Fast molecular-dynamics simulation for ferroelectric thin-film capacitors using a first-principles effective Hamiltonian. *Physical Review B* **2008**, *78* (10), 104104.
37. Paul, J.; Nishimatsu, T.; Kawazoe, Y.; Waghmare, U., A first-principles study of phase transitions in ultrathin films of BaTiO₃. *Pramana* **2008**, *70* (2), 263-270.
38. Paul, J.; Nishimatsu, T.; Kawazoe, Y.; Waghmare, U. V., Polarization switching in epitaxial films of BaTiO₃: A molecular dynamics study. *Applied Physics Letters* **2008**, *93* (24), 242905.
39. Grünebohm, A.; Nishimatsu, T., Influence of defects on ferroelectric and electrocaloric properties of BaTiO₃. *Physical Review B* **2016**, *93* (13), 134101.
40. Qi, Y.; Liu, S.; Grinberg, I.; Rappe, A. M., Atomistic description for temperature-driven phase transitions in BaTiO₃. *Physical Review B* **2016**, *94* (13), 134308.

41. Liu, S.; Grinberg, I.; Rappe, A. M., Development of a bond-valence based interatomic potential for BiFeO₃ for accurate molecular dynamics simulations. *Journal of Physics: Condensed Matter* **2013**, *25* (10), 102202.
42. Shin, Y.-H.; Cooper, V. R.; Grinberg, I.; Rappe, A. M., Development of a bond-valence molecular-dynamics model for complex oxides. *Physical Review B* **2005**, *71* (5), 054104.
43. Shin, Y.-H.; Son, J.-Y.; Lee, B.-J.; Grinberg, I.; Rappe, A. M., Order–disorder character of PbTiO₃. *Journal of Physics: Condensed Matter* **2007**, *20* (1), 015224.
44. Liu, S.; Grinberg, I.; Takenaka, H.; Rappe, A. M., Reinterpretation of the bond-valence model with bond-order formalism: An improved bond-valence-based interatomic potential for PbTiO₃. *Physical Review B* **2013**, *88* (10), 104102.
45. Goddard III, W. A.; Zhang, Q.; Uludogan, M.; Strachan, A.; Cagin, T. In *The ReaxFF polarizable reactive force fields for molecular dynamics simulation of ferroelectrics*, AIP Conference Proceedings, AIP: 2002; pp 45-55.
46. Van Duin, A. C.; Dasgupta, S.; Lorant, F.; Goddard, W. A., ReaxFF: a reactive force field for hydrocarbons. *The Journal of Physical Chemistry A* **2001**, *105* (41), 9396-9409.
47. Chenoweth, K.; Van Duin, A. C.; Goddard, W. A., ReaxFF reactive force field for molecular dynamics simulations of hydrocarbon oxidation. *The Journal of Physical Chemistry A* **2008**, *112* (5), 1040-1053.
48. Mortier, W. J.; Ghosh, S. K.; Shankar, S., Electronegativity-equalization method for the calculation of atomic charges in molecules. *Journal of the American Chemical Society* **1986**, *108* (15), 4315-4320.
49. Senftle, T. P.; Hong, S.; Islam, M. M.; Kylasa, S. B.; Zheng, Y.; Shin, Y. K.; Junkermeier, C.; Engel-Herbert, R.; Janik, M. J.; Aktulga, H. M., The ReaxFF reactive force-field: development, applications and future directions. *npj Computational Materials* **2016**, *2*, 15011.
50. Kowalik, M.; Ashraf, C.; Damirchi, B.; Akbarian, D.; Rajabpour, S.; van Duin, A. C. T., Atomistic Scale Analysis of the Carbonization Process for C/H/O/N-Based Polymers with the ReaxFF Reactive Force Field. *The Journal of Physical Chemistry B* **2019**, *123* (25), 5357-5367.
51. van Duin, A. C. T.; Merinov, B. V.; Han, S. S.; Dorso, C. O.; Goddard, W. A., ReaxFF Reactive Force Field for the Y-Doped BaZrO₃ Proton Conductor with Applications to Diffusion Rates for Multigranular Systems. *Journal of Physical Chemistry A* **2008**, *112* (45), 11414-11422.
52. Kim, S.-Y.; Kumar, N.; Persson, P.; Sofu, J.; van Duin, A. C. T.; Kubicki, J. D., Development of a ReaxFF reactive force field for Titanium dioxide/water systems. *Langmuir* **2013**, *29*, 7838-7846.
53. Vielma, J. M.; Schneider, G., Shell model of BaTiO₃ derived from ab-initio total energy calculations. *Journal of Applied Physics* **2013**, *114* (17), 174108.
54. Liu, S.; Grinberg, I.; Rappe, A. M., Development of a bond-valence based interatomic potential for BiFeO₃ for accurate molecular dynamics simulations. *J Phys Condens Matter* **2013**, *25* (10), 102202.
55. Kwei, G.; Lawson, A.; Billinge, S.; Cheong, S., Structures of the ferroelectric phases of barium titanate. *The Journal of Physical Chemistry* **1993**, *97* (10), 2368-2377.
56. Wang, J. J.; Meng, F. Y.; Ma, X. Q.; Xu, M. X.; Chen, L. Q., Lattice, elastic, polarization, and electrostrictive properties of BaTiO₃ from first-principles. *Journal of Applied Physics* **2010**, *108* (3), 034107.
57. Fechner, M.; Ostanin, S.; Mertig, I., Effect of the surface polarization in polar perovskites studied from first principles. *Physical Review B* **2008**, *77* (9), 094112.
58. Kay, H. F.; Vousden, P., XCV. Symmetry changes in barium titanate at low temperatures and their relation to its ferroelectric properties. *The London, Edinburgh, and Dublin Philosophical Magazine and Journal of Science* **1949**, *40* (309), 1019-1040.
59. Hellwege, K.; Hellwege, A., Ferroelectrics and related substances, Landolt-Börnstein, New Series. *Group III* **1969**, *3*.

60. Wieder, H., Electrical behavior of barium titanate single crystals at low temperatures. *Physical Review* **1955**, *99* (4), 1161.
61. Shirane, G.; Takeda, A., Transition energy and volume change at three transitions in barium titanate. *Journal of the Physical Society of Japan* **1952**, *7* (1), 1-4.
62. Zhao, Z.; Buscaglia, V.; Viviani, M.; Buscaglia, M. T.; Mitoseriu, L.; Testino, A.; Nygren, M.; Johnsson, M.; Nanni, P., Grain-size effects on the ferroelectric behavior of dense nanocrystalline BaTiO₃ ceramics. *Physical Review B* **2004**, *70* (2), 024107.
63. Junquera, J.; Ghosez, P., Critical thickness for ferroelectricity in perovskite ultrathin films. *Nature* **2003**, *422* (6931), 506.
64. Tenne, D. A.; Turner, P.; Schmidt, J.; Biegalski, M.; Li, Y.; Chen, L.; Soukiasian, A.; Trolier-McKinstry, S.; Schlom, D.; Xi, X., Ferroelectricity in ultrathin BaTiO₃ films: probing the size effect by ultraviolet Raman spectroscopy. *Physical review letters* **2009**, *103* (17), 177601.
65. Li, K. T.; Lo, V. C., Simulation of thickness dependence in ferroelectric thin films. *Solid state communications* **2004**, *132* (1), 49-54.
66. Wang, X.; Deng, X.; Wen, H.; Li, L., Phase transition and high dielectric constant of bulk dense nanograin barium titanate ceramics. *Applied physics letters* **2006**, *89* (16), 162902.
67. Li, Y.; Yu, R.; Zhou, H.; Cheng, Z.; Wang, X.; Li, L.; Zhu, J., Direct observation of thickness dependence of ferroelectricity in freestanding BaTiO₃ thin film. *Journal of the American Ceramic Society* **2015**, *98* (9), 2710-2712.
68. Cockayne, E.; Burton, B. P., Dipole moment of a Pb-O vacancy pair in PbTiO₃. *Physical Review B* **2004**, *69* (14), 144116.
69. Tselev, A.; Ganesh, P.; Qiao, L.; Siemons, W.; Gai, Z.; Biegalski, M. D.; Baddorf, A. P.; Kalinin, S. V., Oxygen control of atomic structure and physical properties of SrRuO₃ surfaces. *ACS nano* **2013**, *7* (5), 4403-4413.
70. Zhang, Y.; Li, J.; Fang, D., Oxygen-vacancy-induced memory effect and large recoverable strain in a barium titanate single crystal. *Physical Review B* **2010**, *82* (6), 064103.
71. Tufte, O.; Chapman, P., Electron mobility in semiconducting strontium titanate. *Physical Review* **1967**, *155* (3), 796.
72. Ren, X., Large electric-field-induced strain in ferroelectric crystals by point-defect-mediated reversible domain switching. *Nature materials* **2004**, *3* (2), 91.
73. Lopez-Bezanilla, A.; Ganesh, P.; Littlewood, P. B., Magnetism and metal-insulator transition in oxygen-deficient SrTiO₃. *Physical Review B* **2015**, *92* (11), 115112.
74. Zhuang, H. L.; Ganesh, P.; Cooper, V. R.; Xu, H.; Kent, P., Understanding the interactions between oxygen vacancies at SrTiO₃ (001) surfaces. *Physical Review B* **2014**, *90* (6), 064106.
75. Gangopadhyay, S.; Masunov, A. E.; Inerbaev, T.; Mesit, J.; Guha, R. K.; Sleiti, A. K.; Kapat, J. S., Understanding oxygen vacancy migration and clustering in barium strontiumcobalt iron oxide. *Solid State Ionics* **2010**, *181* (23-24), 1067-1073.
76. Erhart, P.; Albe, K., Thermodynamics of mono- and di-vacancies in barium titanate. *Journal of Applied Physics* **2007**, *102* (8), 084111.
77. Li, M.; Li, J.; Chen, L.-Q.; Gu, B.-L.; Duan, W., Effects of strain and oxygen vacancies on the ferroelectric and antiferrodistortive distortions in PbTiO₃/SrTiO₃ superlattice. *Physical Review B* **2015**, *92* (11), 115435.
78. Bednyakov, P. S.; Sluka, T.; Tagantsev, A. K.; Damjanovic, D.; Setter, N., Formation of charged ferroelectric domain walls with controlled periodicity. *Scientific reports* **2015**, *5*, 15819.
79. Li, X.; Wang, B.; Zhang, T.-Y.; Su, Y., Water adsorption and dissociation on BaTiO₃ single-crystal surfaces. *The Journal of Physical Chemistry C* **2014**, *118* (29), 15910-15918.

80. He, D.; Qiao, L.; Khodayari, M.; Volinsky, A. A., Electric field and humidity effects on adsorbed water behavior on BaTiO₃ ferroelectric domains studied by scanning probe microscopy. *Journal of Applied Physics* **2014**, *116* (8), 084105.
81. Yasui, K.; Kato, K., Influence of adsorbate-induced charge screening, depolarization factor, mobile carrier concentration, and defect-induced microstrain on the size effect of a BaTiO₃ nanoparticle. *The Journal of Physical Chemistry C* **2013**, *117* (38), 19632-19644.
82. Li, X.; Bai, Y.; Wang, B.; Su, Y., Water adsorption induced in-plane domain switching on BaTiO₃ surface. *Journal of Applied Physics* **2015**, *118* (9), 094104.